

A General Model to Calculate the Spin-Lattice Relaxation Rate (R1) of Blood, Accounting for Hematocrit, Oxygen Saturation, Oxygen Partial Pressure, and Magnetic Field Strength Under Hyperoxic Conditions

Emma Bluemke, BS,*  Eleanor Stride, PhD, and Daniel P. Bulte, PhD

Background: Under normal physiological conditions, the spin-lattice relaxation rate (R1) in blood is influenced by many factors, including hematocrit, field strength, and the paramagnetic effects of deoxyhemoglobin and dissolved oxygen. In addition, techniques such as oxygen-enhanced magnetic resonance imaging (MRI) require high fractions of inspired oxygen to induce hyperoxia, which complicates the R1 signal further. A quantitative model relating total blood oxygen content to R1 could help explain these effects.

Purpose: To propose and assess a general model to estimate the R1 of blood, accounting for hematocrit, SO_2 , PO_2 , and B_0 under both normal physiological and hyperoxic conditions.

Study Type: Mathematical modeling.

Population: One hundred and twenty-six published values of R1 from phantoms and animal models.

Field Strength/Sequence: 5–8.45 T.

Assessment: We propose a two-compartment nonlinear model to calculate R1 as a function of hematocrit, PO_2 , and B_0 . The Akaike Information Criterion (AIC) was used to select the best-performing model with the fewest parameters. A previous model of R1 as a function of hematocrit, SO_2 , and B_0 has been proposed by Hales et al, and our work builds upon this work to make the model applicable under hyperoxic conditions ($SO_2 > 0.99$). Models were assessed using the AIC, mean squared error (MSE), coefficient of determination (R^2), and Bland–Altman analysis. The effect of volume fraction constants W_{RBC} and W_{plasma} was assessed by the SD of resulting R1. The range of the model was determined by the maximum and minimum B_0 , hematocrit, SO_2 , and PO_2 of the literature data points.

Statistical Tests: Bland–Altman, AIC, MSE, coefficient of determination (R^2), SD.

Results: The model estimates agreed well with the literature values of R1 of blood ($R^2 = 0.93$, $MSE = 0.0013 \text{ s}^{-2}$), and its performance was consistent across the range of parameters: $B_0 = 1.5\text{--}8.45 \text{ T}$, $SO_2 = 0.40\text{--}1$, $PO_2 = 30\text{--}700 \text{ mmHg}$.

Data Conclusion: Using the results from this model, we have quantified and explained the contradictory decrease in R1 reported in oxygen-enhanced MRI and oxygen-delivery experiments.

Level of Evidence: 3

Technical Efficacy: Stage 1

J. MAGN. RESON. IMAGING 2022;55:1428–1439.

As quantitative MRI techniques grow in popularity, the ability to accurately estimate the spin-lattice relaxation time constant (T1) or relaxation rate ($R1 = 1/T1$) is becoming increasingly important. For example, an accurate estimate

View this article online at [wileyonlinelibrary.com](https://onlinelibrary.wiley.com/doi/10.1002/jmri.27938). DOI: 10.1002/jmri.27938

Received May 21, 2021, Accepted for publication Sep 18, 2021.

*Address reprint requests to: E.B., Headington, Oxford, Oxfordshire OX3 7DQ, UK. E-mail: emma.bluemke@new.ox.ac.uk
[Correction added on 23 October 2021, after first online publication: Equations (8) and (11) have been corrected in this version.]

From the Department of Engineering Sciences, Institute of Biomedical Engineering, University of Oxford, Oxford, UK

Additional supporting information may be found in the online version of this article

This is an open access article under the terms of the Creative Commons Attribution License, which permits use, distribution and reproduction in any medium, provided the original work is properly cited.

of R1 in blood is important for several research techniques such as arterial spin labeling and black blood imaging.^{1,2} Under normal physiological conditions, the relaxation rate in blood is influenced by many factors, including hematocrit, field strength, temperature, protein concentrations, and the weak paramagnetic effects of deoxyhemoglobin and dissolved oxygen in the plasma.^{3–5} In addition, evolving techniques such as oxygen-enhanced magnetic resonance imaging (MRI) require high fractions of inspired oxygen to induce hyperoxia, which complicates the R1 signal further.^{6–11} Whilst a linear increase in R1 with oxygen partial pressure has been reported in phantom experiments, measurements in blood have produced contradictory effects, in some cases showing an unexpected decrease in R1 following induction of hyperoxia.¹²

In response to these contradictory results, a recent *Journal of Magnetic Resonance Imaging* Editorial by Desmond et al suggests that “future work could expand the interpretation of the T1 and T2* changes using quantitative models relating total blood oxygen content, partial pressure of oxygen (PO₂) and oxygen saturation (SO₂) to the MRI measures.”¹³ Existing models for predicting R1 in blood can account for SO₂, hematocrit, and magnetic field strength, but are not applicable under conditions of artificially increased PO₂, or hyperoxic experiments.¹⁴ Therefore, in this paper our aim was to establish a general model that could estimate the R1 of blood, accounting for hematocrit, SO₂, PO₂, and magnetic field strength under both normal physiological and hyperoxic conditions.

Materials and Methods

Background Theory

The relationship between longitudinal relaxation and the paramagnetism of oxygen in blood has a long history in MRI, beginning when Young et al¹⁵ and Tripathi et al¹⁶ found that increasing inspired oxygen fractions led to a small but definite increase in the R1 of blood in the left ventricle (i.e., oxygenated blood), but no change in R1 in the right ventricle (i.e., deoxygenated blood). To identify the physiology underlying these contrast changes, experiments using the vitreous fluid of the eye¹⁷ and ex vivo blood samples at varying levels of oxygenation led to the hypothesis that the paramagnetic dissolved oxygen in the plasma provides the contrast during hyperoxia.¹⁸ This hypothesis was confirmed in ex vivo blood samples by d’Othée et al,⁵ where measurements of the *bound* and *dissolved* oxygen plotted alongside the measured R1 (reproduced in Fig. S1 in the Supplemental Material) showed that following full oxygen saturation, the R1 of blood increases linearly with increasing dissolved oxygen, while the bound oxygen remains constant. Prior to full oxygen saturation, however, experiments by Silvennoinen et al showed that the main source of contrast change is caused by changing levels of paramagnetic deoxyhemoglobin, where R1 decreased linearly as SO₂ increased (i.e., with decreasing deoxyhemoglobin concentration).⁴

In 2016, Hales et al published a general model to calculate the spin–lattice relaxation time constant (T1) of blood, accounting for hematocrit, SO₂, and magnetic field strength.¹⁴ The model built

upon a two-compartment model proposed by Grgac et al, in which a fast-exchange model¹⁹ model was used to describe blood R1 because the water exchange rate between the plasma and cytoplasm is faster than the difference in R1 between these two compartments,^{20–22} given by:

$$R1_b(SO_2) = f_e R1_e SO_2 + (1 - f_e) R1_p, \quad (1)$$

where R1_b is the relaxation rate of whole blood, SO₂ is the oxygen saturation fraction (range of 0–1), R1_p is the longitudinal relaxation rate of plasma (s^{−1}), and R1_e is the longitudinal relaxation rate of erythrocytes (s^{−1}).

The variable f_e is the fraction of water in whole blood that resides in erythrocytes (0–1), which is described by the equation:

$$f_e(Hct) = \frac{W_{RBC} Hct}{W_{RBC} Hct + W_{plasma} (1 - Hct)}, \quad (2)$$

where Hct is the hematocrit (range of 0–1), W_{RBC} is the volume fraction of water within the erythrocyte (typically valued at 0.70 due to hemoglobin occupying approximately 30% of the erythrocyte volume), and W_{plasma} is the volume fraction of water within the plasma (typically valued at 0.95, where the other 5% volume is occupied by plasma proteins such as albumin).²¹

Hales et al extended this model to account for the effect that deoxyhemoglobin has on R1_e, as a paramagnetic contrast agent, expressing R1_e as a function of SO₂:

$$R1_e(SO_2) = R1_{cox} + r1_{dHb} [Hb] (1 - SO_2), \quad (3)$$

where R1_{cox} is the relaxation rate of erythrocytes when SO₂ = 100%, [Hb] is the mean corpuscular hemoglobin concentration (5.15 mmol Hb tetramer/L plasma), and r1_{dHb} is the molar relaxivity of deoxyhemoglobin (in s^{−1} L plasma in erythrocyte/mmol Hb tetramer).

Combining Eqs. 1–3 results in the following model for calculating R1 of blood (Eq. 4):

$$R1_b(SO_2) = f_e (R1_{cox} + r1_{dHb} [Hb] (1 - SO_2)) + (1 - f_e) R1_p. \quad (4)$$

In addition, Hales et al modeled R1_{cox}, R1_p, and r1_{dHb} to have a linear dependence on B0 (where β_0 and β_1 are the y-intercept and slope for the linear fit):

$$R1_{cox}(B0) = \beta_{0,R1_{cox}} + \beta_{1,R1_{cox}} B0 \quad (5)$$

$$R1_p(B0) = \beta_{0,R1_p} + \beta_{1,R1_p} B0 \quad (6)$$

$$r1_{dHb}(B0) = \beta_{0,r1_{dHb}} + \beta_{1,r1_{dHb}} B0 \quad (7)$$

Hales et al fitted this model to 42 data points from the literature with R1 measured at various Hct, SO₂, and B0 (1.5–7 T). If the data were not acquired at 37 °C or in vivo, the T1 values were increased to account for the shift in R1 caused by the difference in temperature (by 12% for a shift from 22 °C to 37

°C, as done by Hales et al). From this model and subset of data, Hales et al obtained values for the five parameters $\beta_{0,R1_{\text{cox}}}$, $\beta_{1,R1_{\text{cox}}}$, $\beta_{0,r1_{\text{dHb}}}$, $\beta_{0,R1_{\text{p}}}$, and $\beta_{1,R1_{\text{p}}}$. In the fitting process performed by Hales et al, $\beta_{1,r1_{\text{dHb}}}$ was found to be almost zero and the authors concluded that $r1_{\text{dHb}}$ was not dependent on field strength.

New Model

The fitted value for $r1_{\text{dHb}}$ of $0.033 \text{ (s}^{-1} \text{ L plasma in erythrocyte/mmole Hb tetramer)}$ from Hales et al lies between the mean fitted values of 0.052 and $0.012 \text{ (s}^{-1} \text{ L plasma in erythrocyte/mmole Hb tetramer)}$ as estimated previously.^{3,20} However, these estimates do not agree with empirical results from Silvennoinen et al,⁴ who from their data, estimated that the R1 in erythrocytes decreased with oxygenation level linearly with the equation $1.46 - 0.60 \text{ s}^{-1} \text{ SO}_2$. When divided by $5.15 \text{ [mmole Hb tetramer/L plasma]}$, the $r1_{\text{dHb}}$ is $-0.117 \text{ [s}^{-1} \text{ L plasma in erythrocyte/mmole Hb tetramer]}$, which has a greater effect on R1 than the $r1_{\text{dHb}}$ estimated by Hales et al. This disagreement is likely explained by a key limitation of Eq. 4, i.e., that there is no parameter accounting for the change in plasma R1 ($R1_{\text{p}}$) caused by increasing PO_2 due to changing SO_2 .

To address this limitation, we defined a new parameter, $r1_{\text{pOx}}$, the relaxivity of dissolved oxygen in the plasma in $\text{s}^{-1}/\text{mmHg oxygen}$ (Eq. 8), which we modeled as having a linear dependence on field strength (Eq. 9) in the same manner as Hales et al had for $r1_{\text{dHb}}$, $R1_{\text{cox}}$, and $R1_{\text{p}}$ (Eqs. 5–7):

$$R1_{\text{b}}(\text{SO}_2, \text{PO}_2) = f_e (R1_{\text{cox}} + r1_{\text{dHb}}[\text{Hb}](1 - \text{SO}_2)) + (1 - f_e)(R1_{\text{p}} + r1_{\text{pOx}}\text{PO}_2) \quad (8)$$

$$r1_{\text{pOx}}(B0) = \beta_{0,r1_{\text{pOx}}} + \beta_{1,r1_{\text{pOx}}} B0. \quad (9)$$

Although we model Eqs. 5–7 and 9 as linear, the true relationship between field strength and both R1 and the relaxivity ($r1$) is nonlinear and depends on the material.^{23–25} For R1, protons in highly mobile molecules such as water or plasma will be less affected by changing field strength, whereas in materials such as biological tissues the R1 has been empirically shown to decrease as field strength increases by approximately $B0^{-1/3}$ (see Fig. S2a in the Supplemental Material).²³ However, when examined from the range of 1.5 – 7 T , measurements by Rooney et al (provided in Fig. S2b in the Supplemental Material) suggest that using a linear model for $R1_{\text{cox}}$ ($B0$) (Eq. 5) and $R1_{\text{p}}$ ($B0$) (Eq. 6) is appropriate in the field strength range of this model (1.5 – 8.45 T). Similarly, an experiment by Chou et al measured the relaxivity ($r1$) of paramagnetic contrast agents over a large range of field strengths (0 – 12 T), revealing a Lorentzian shape (reproduced in Fig. S3a in the Supplemental Material).²⁴ However, when only examined between the range of 1.5 – 8.45 T , the measurements by Chou et al (provided in Fig. S3b in the Supplemental Material) suggest that using a linear model for $r1_{\text{dHb}}$ ($B0$) (Eq. 7) and $r1_{\text{pOx}}$ ($B0$) (Eq. 9) is appropriate in the field strength range used in this model (1.5 – 8.45 T). Therefore, a linear model has been chosen for Eq. 5–7 and 9.

Equation 8 is a function of both SO_2 and PO_2 , which can be related by the invertible form of the hemoglobin-oxygen dissociation curve (the Hill equation)²⁶:

$$\text{SO}_2(\text{PO}_2) = \frac{\text{PO}_2^n}{\text{PO}_2^n + P50^n}, \quad (10)$$

where $P50$ is the half-saturation PO_2 and n is the Hill exponent for hemoglobin (typically 2.7).²⁷ $P50$ will vary by species and can be set to match the species of interest by using values obtained experimentally.²⁶ By substituting Eq. 10 into Eq. 8, we obtain Eq. 11 for calculating the R1 of blood that is no longer limited to normal physiological oxygen ranges. Thus, Eq. 11 can be used to calculate R1 even when the partial pressure of oxygen in the plasma reaches normobaric hyperoxic levels.

$$R1_{\text{b}}(\text{PO}_2) = f_e \left(R1_{\text{cox}} + r1_{\text{dHb}}[\text{Hb}] \left(1 - \frac{\text{PO}_2^n}{\text{PO}_2^n + P50^n} \right) \right) + (1 - f_e)(R1_{\text{p}} + r1_{\text{pOx}}\text{PO}_2). \quad (11)$$

In addition, it is known that many paramagnetic contrast agents interact with macromolecules and exhibit a higher relaxivity at higher macromolecule concentrations.²⁸ This is also true for molecular oxygen, and blood with artificially high levels of hematocrit ($\text{Hct} = 0.6$) has been shown to have a higher relaxivity than blood at regular hematocrit levels.²⁹ To account for this hematocrit sensitivity, we also tested the effect of adding an extra term, $\beta_{1,r1_{\text{pOxHct}}}$, to Eq. 9, assuming a linear dependence on hematocrit.

Data Analysis

In order to estimate values for the parameters in the new model, 126 data points for R1 in blood were collected from the literature with measured or estimated Hct, SO_2 , and PO_2 at a range of field strengths (1.5 – 9 T) and under normoxic and hyperoxic conditions (Table 1).^{3,5,20,29–34} Data were extracted either from tables, manuscript text or graphs, and if data extraction from graphs was necessary, a digital plot analyzer was used to reliably extract values.³⁵ The distribution of the resulting data is shown in Fig. S4 in the Supplemental Material. An accurate measurement of T1 depends on the selection of acquisition protocols and parameters (such as repetition and inversion times), and therefore the acquisition details from each experiment are listed in Table S1 in the Supplemental Material.

The T1 values from Stefanovic and Pike and d'Othée et al were increased by 12% to account for the shift in T1 between 22°C and 37°C .^{10,35} If not reported, PO_2 values were calculated from the reported SO_2 values using Eq. 9. Since the value of $P50$ (half-saturation PO_2) can differ greatly between species, a $P50$ of 25 mmHg was used for all human data points, and a $P50$ of 44 mmHg was used for the bovine and rat, based on the $P50$ values found experimentally in human, bovine, and rat blood samples.²⁶

For model fitting, the SciPy *optimize* function for nonlinear least-squares fitting was used.³⁶ Equation 11 was fitted using a randomized subset of 95% of the 126 data points, fitting with the R1, $B0$, $P50$, Hct, and PO_2 values simultaneously, and testing on the

TABLE 1. Summary of the Literature Sources for the Data Used to Parameterize the New Model

Reference	B0 (T)	N	Blood Source	Hematocrit	SO ₂ (%)	PO ₂ (mmHg)	Temp (°C)	Normal or Hyperoxic
Lu ³⁰	3	9	Bovine blood ex vivo	Measured	Measured	Calculated	37	Normal
Grgac ²⁰	7	20		Measured	Measured	Calculated	37	Normal
Dobre ³¹	4.7	1		Measured	Measured	Calculated	37	Normal
	7	1						
	9	1						
d'Othée ⁵	8.45	11		Measured	Measured	Measured	22	Hyperoxic
	3	7						
Pilkinton ³²	3	5	Rat blood in vivo	Estimated	Calculated	Measured	In vivo	Hyperoxic
Blockley ³	1.5	11	Human Blood ex vivo	Measured	Measured	Calculated	37	Normal
	3	7						
	7	11						
Hueckel ²⁹	1.5	17		Measured	Calculated	Measured	37	Hyperoxic
Stefanovic ³³	1.5	8		Measured	Measured	Calculated	22	Normal
Rane ³⁴	7	10		Measured	Measured	Calculated	37	Normal
Summary: Total data range	1.5–9	Total # of data points N = 126	Human N = 64, bovine N = 58, rat N = 5	Total Hct range of 0–1	Total SO ₂ range of 42– 100%	Total PO ₂ range of 33– 739 mmHg	All R1 values corrected to 37 °C	86 data points normal, 40 data points hyperoxic

The distribution of the data points is plotted in Fig. S1 in the Supplemental Material. The MRI acquisition details from each experiment are listed in Table S1 in the Supplemental Material.

TABLE 2. A Summary of the Final Parameter Estimates from the Model Fitting

Parameter Meaning	Parameter Name	Mean Parameter Value (95% Lower and Upper Confidence Intervals)		Units
		Hales 2016 Parameters	New Model Parameters	
The Y-intercept of the linear dependence on B0 for the $R1_{\text{cox}}$, the relaxation rate of erythrocytes when $\text{SO}_2 = 100\%$	$\beta_{0,R1\text{cox}}$	1.10 (0.97, 1.28)	1.237 (1.221, 1.252)	s^{-1}
The slope of the linear dependence on B0 for the $R1_{\text{cox}}$, the relaxation rate of erythrocytes when $\text{SO}_2 = 100\%$	$\beta_{1,R1\text{cox}}$	−0.058 (−0.085, −0.038)	−0.0825 (−0.0854, −0.0796)	$\text{s}^{-1} \text{ T}^{-1}$
The Y-intercept of the linear dependence on B0 for the $r1_{\text{dHb}}$, which is the molar relaxivity of deoxyhemoglobin	$\beta_{0,r1\text{dHb}}$	0.033 (1.8×10^{-9} , 0.056)	0.102 (0.093, 0.110)	$\text{s}^{-1} \text{ L plasma in erythrocyte/mmole Hb tetramer}$
The slope of the linear dependence on B0 for the $r1_{\text{dHb}}$, which is the molar relaxivity of deoxyhemoglobin	$\beta_{1,r1\text{dHb}}$	Not used—set to 0	−0.00688 (−0.00853, −0.00523)	$\text{s}^{-1} \text{ T}^{-1} \text{ L plasma in erythrocyte/mmole Hb tetramer}$
The Y-intercept of the linear dependence on B0 for $R1_{\text{p}}$, the longitudinal relaxation rate of plasma	$\beta_{0,R1\text{p}}$	0.49 (0.40, 0.57)	0.332 (0.326, 0.337)	s^{-1}
The slope of the linear dependence on B0 for $R1_{\text{p}}$, the longitudinal relaxation rate of plasma	$\beta_{1,R1\text{p}}$	−0.023 (−0.035, −0.0079)	Not used—set to 0	$\text{s}^{-1} \text{ T}^{-1}$
The Y-intercept of the linear dependence on B0 for $r1_{\text{pOx}}$, the relaxivity of dissolved oxygen in the plasma	$\beta_{0,r1\text{pOx}}$	Not tested	5.70×10^{-4} (5.87×10^{-4} , 8.95×10^{-5})	$\text{s}^{-1}/\text{mmHg}$
The slope of the linear dependence on B0 for $r1_{\text{pOx}}$, the relaxivity of dissolved oxygen in the plasma	$\beta_{1,r1\text{pOx}}$	Not tested	-3.86×10^{-5} (-4.27×10^{-5} , -3.56×10^{-5})	$\text{s}^{-1} \text{ T}^{-1}/\text{mmHg}$

remaining 5%. The dataset was split for fitting and testing using the SciKitLearn *train_test_fit* function with shuffling.³⁷ This process was iterated 10,000 times, and the mean and 95% confidence interval of the distribution of fitted values for each of the parameters were recorded (listed in Table 2).

Effect of W_{RBC} and W_{plasma} Constants

In Eq. 2, the values used for W_{RBC} and W_{plasma} were 0.70 and 0.95, respectively. Experimentally, W_{RBC} has been measured to be at maximum 78% and at minimum 54%,³⁸ and 94% has sometimes been used for W_{plasma} instead of 95%.⁴ To examine the effect of this range of possible variables on the final R1, the resulting R1 was

calculated for all combinations of $W_{\text{RBC}} = 54\text{--}78\%$ and $W_{\text{plasma}} = 94\text{--}96\%$, and Hct = 0.38–48.

Statistical Analysis

Since Eq. 11 contains eight fitting parameters, the fitting process was repeated for all combinations of fewer parameters (i.e., removing the dependence of $R1_{\text{p}}$ on B0), and the Akaike Information Criterion (AIC) was calculated for each version of the model—the best-fit model according to the AIC is the model that explains the greatest amount of variation using the fewest possible independent variables. The model that scored the highest according to the AIC was therefore selected as the best model and used in further investigation. The R^2 coefficient of determination and mean squared error (MSE)

were also calculated for each model, and Bland–Altman analysis was used to examine the model bias with hematocrit, B0, SO₂, and PO₂.

After the resulting R1 was calculated for all combinations of $W_{\text{RBC}} = 54\text{--}78\%$ and $W_{\text{plasma}} = 94\text{--}96\%$, and Hct = 0.38–48, the mean and SD of the R1 values were calculated to examine the effect of the W_{RBC} and W_{plasma} constants.

Results

Akaike Information Criterion

The AIC score, R^2 , and MSE results of the four highest AIC-scoring models tested are listed in Table S2 in the

Supplemental Material, and results are plotted in Fig. S5 in the Supplemental Material. The version of the model with $\beta_{1,\text{R1P}}$ set to 0 (i.e., with Eq. 6 set to $\text{R1}_p = \beta_{0,\text{R1P}}$, hence 7 total parameters) resulted in the highest AIC score, and was therefore used in this manuscript.

The version of the model with the extra fitting parameter $\beta_{1,\text{r1pOxHct}}$ in Eq. 9 resulted in a similar fit ($R^2 = 0.927$ vs. $R^2 = 0.926$), but the best-fit model according to the AIC was the model without this extra parameter (see Table S2 in the Supplemental Material). Therefore, the best model was the 7-parameter model which did not include this dependency on hematocrit.

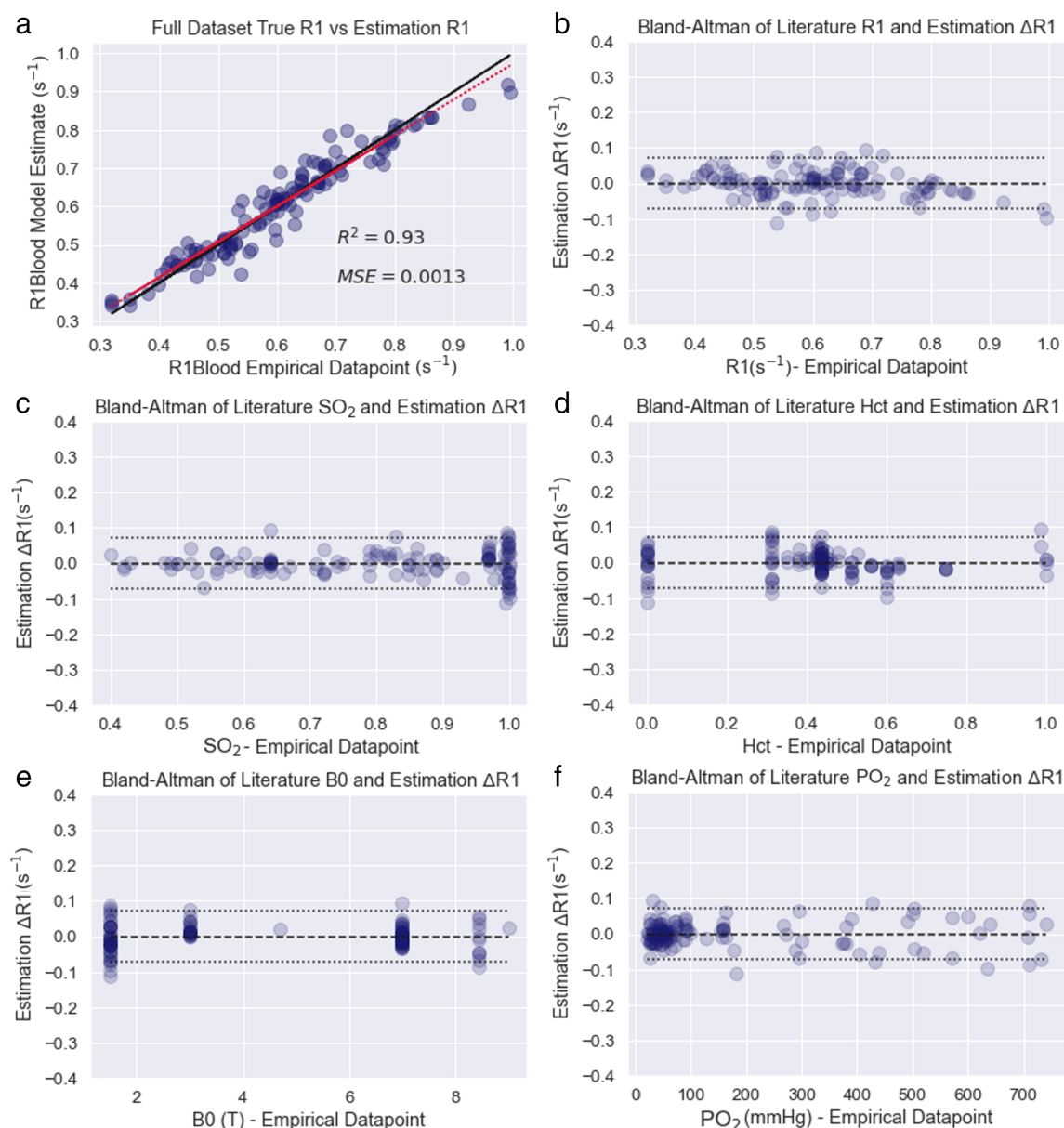


FIGURE 1: (a) The modeled vs. measured R1_b values, plotted against the line of equality (solid black line) and a linear regression (red dotted line, $R^2 = 0.93$), number of datapoints $N = 126$. (b) A Bland–Altman plot showing the difference between the modeled and measured values of R1_b . The horizontal long-dashed lines show the mean value of ΔR1_b ($6 \times 10^{-6} \text{ s}^{-1}$), and the horizontal dotted lines show the limits of agreement (long dashes, calculated by $\text{mean}(\Delta\text{R1}_b) \pm (1.96 \times \text{SD}(\Delta\text{R1}_b))$). Bland–Altman plots for the error in modeled R1_b against (c) SO₂, (d) hematocrit, (e) B0, and (f) PO₂ levels are also shown to examine bias in the model.

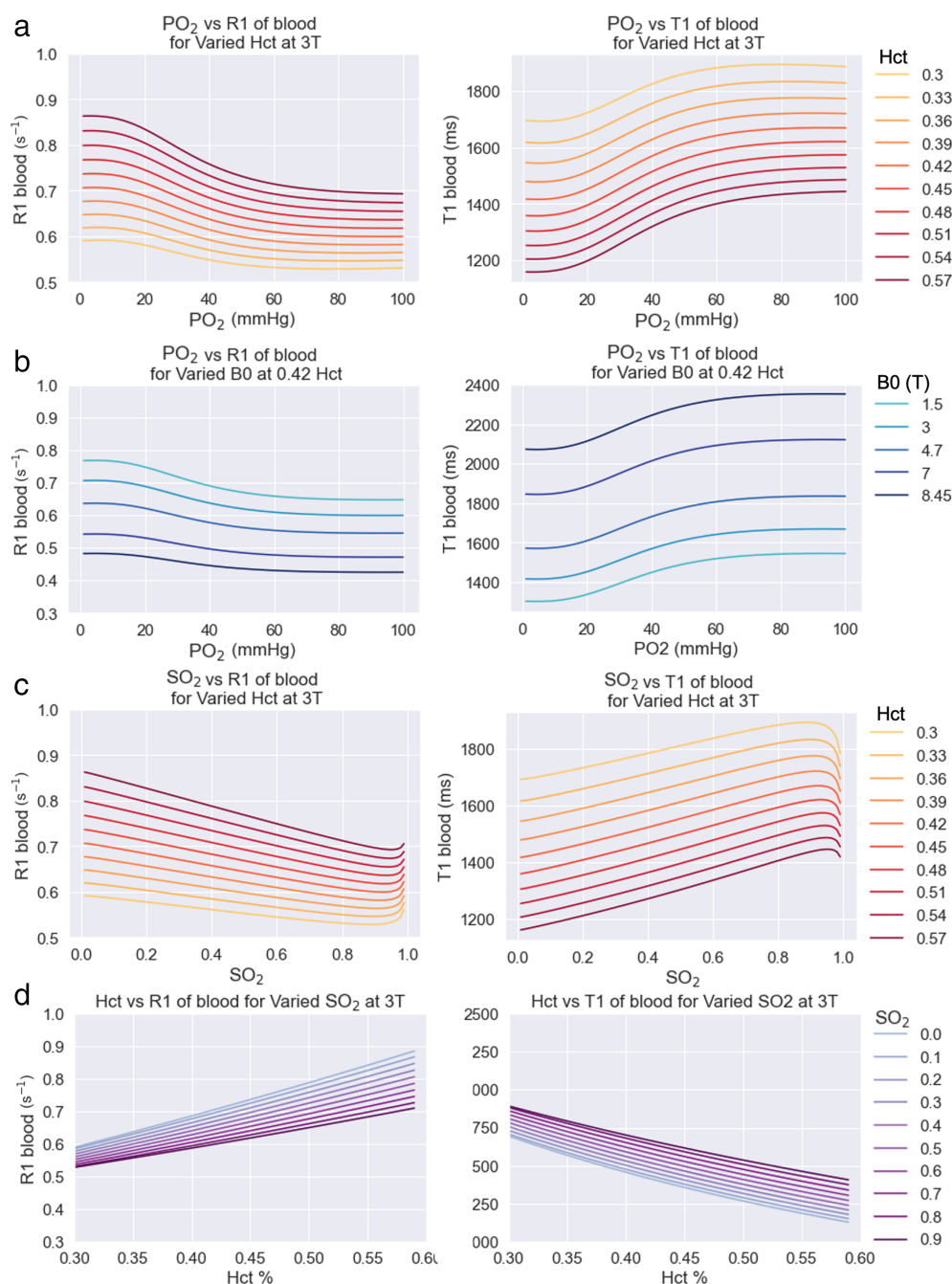


FIGURE 2: Plots with simulated data to illustrate the behavior of the model (with parameters fit from all data) under non-hyperoxic conditions ($\text{SO}_2 < 99\%$). (a) PO_2 vs. R1_b and T1_b and (b) SO_2 vs. R1_b and T1_b for a range of hematocrit values (0.3–0.57) at 3 T. (c) PO_2 vs. R1_b and T1_b at a range of field strengths (1.5–7 T) with $\text{Hct} = 0.42$. (d) Hematocrit vs. R1_b and T1_b for a range of SO_2 values (0–90%) at 3 T.

Model Fitting

The modeled vs. measured R1_b values from the randomized unseen test set of each iteration are plotted in Fig. S6 in the Supplemental Material alongside the line of equality and the linear regression ($R^2 = 0.91$). The difference between the modeled and measured R1_b values from the randomized unseen test set of each iteration is illustrated as Bland–Altman plots in Fig. S6b–f in the Supplemental Material with the resulting mean error of R1_{blood} as $1 \times 10^{-4} \text{ s}^{-1}$ and the

limits of agreement of -0.078 s^{-1} and 0.078 s^{-1} . Violin plots showing the distribution of parameter estimates from each iteration are shown in Fig. S7 in the Supplemental Material.

The median parameter values for the final optimal 7 parameters $\beta_{0,\text{R1eox}}$, $\beta_{1,\text{R1eox}}$, $\beta_{0,\text{r1dHb}}$, $\beta_{1,\text{r1dHb}}$, $\beta_{0,\text{R1p}}$, $\beta_{0,\text{r1pOx}}$, and $\beta_{1,\text{r1pOx}}$ (with lower and upper 95% confidence intervals) are listed in Table 2. The accuracy of the final model's predicted R1 compared against the “true” R1_b values

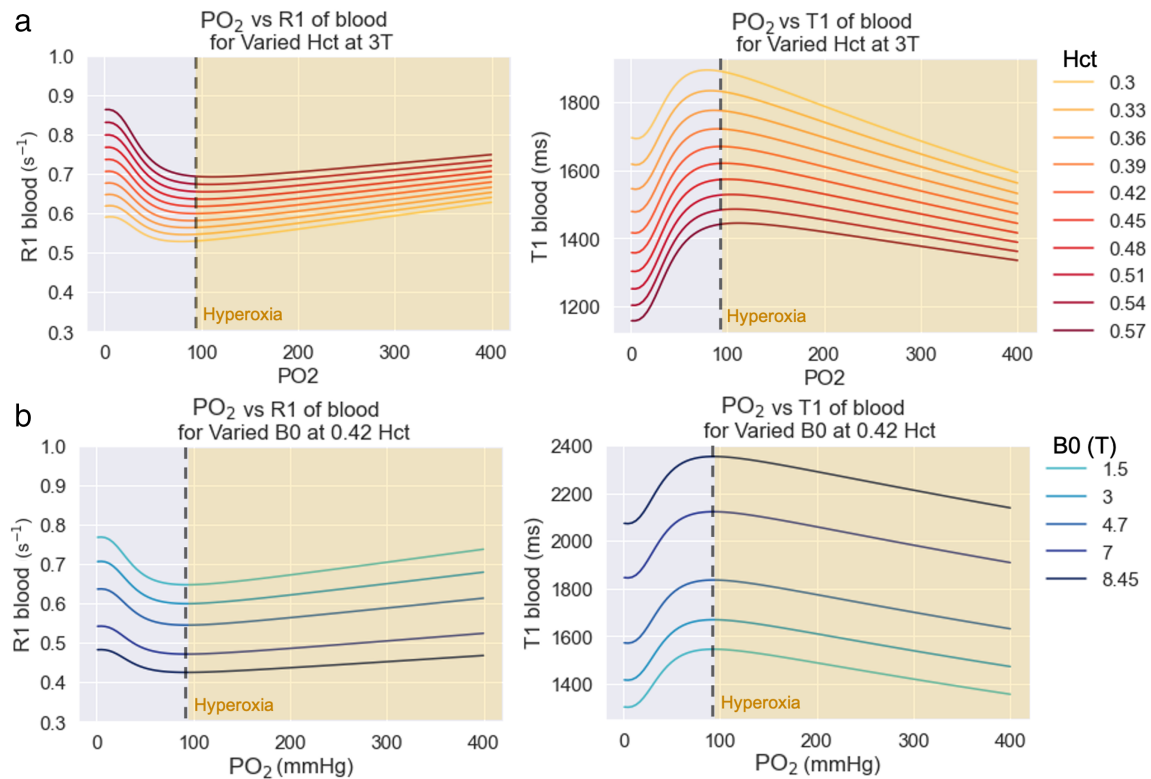


FIGURE 3: Plots with simulated data to illustrate the behavior of the model extending to hyperoxic conditions. (a) PO₂ vs. R1_b and T1_b for a range of hematocrit values (0.3–0.57) at 3 T. (b) PO₂ vs. R1_b and T1_b for a range of field strengths (1.5–8.45 T) at 0.42 Hct.

is shown in Fig. 1a. The predicted vs. true R1_b values are plotted against the line of equality (solid black line) and a linear regression (dotted line, $R^2 = 0.93$) in Fig. 1a, with a final MSE of 0.0013 s^{-2} . To examine bias in the model with respect to SO₂, PO₂, B0, Hct, or R1 variables, Bland–Altman plots are provided in Fig. 1b–f, with the resulting mean error of R1_{blood} as $6 \times 10^{-6} \text{ s}^{-1}$ and the limits of agreement of -0.071 s^{-1} and 0.071 s^{-1} . A systematic trend in the error distribution by R1 (Fig. 1b) indicated that the model did not entirely explain the non-noise variance in the data, and possible causes of this were further examined by viewing the datapoints according to the original source (provided in Fig. S8 in the Supplemental Material).

Model Behavior

To understand the behavior of the resulting model, the effect of varying PO₂, SO₂, field strength, and hematocrit on R1 is illustrated using synthetic data from 0 to the upper level of normal oxygen levels (Fig. 2) and extending to hyperoxic conditions (Fig. 3).

As shown in Fig. 4, the ability of the new model to predict blood R1 was compared with the model and parameter values estimated by Hales et al, on a subset of data points ($N = 128$) from non-hyperoxic blood, i.e., within the range that the Hales model is stated to be valid (SO₂ = 0.4–0.99). Within this range, the model agreed well with the Hales model estimates of R1 ($R^2 = 0.96$), and showed slightly

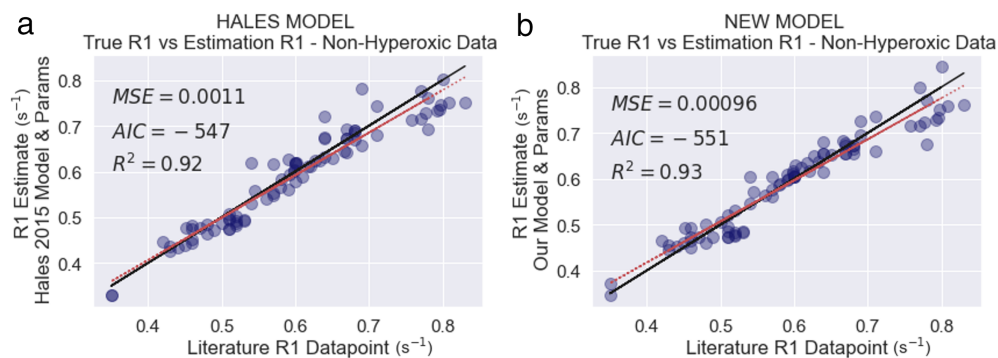


FIGURE 4: Scatterplots of a subset of 82 literature data points from non-hyperoxic blood (SO₂ < 99%) and the performance of (a) the model and parameters estimated by Hales et al ($R^2 = 0.92$, MSE = 0.0011 s^{-2} , AIC = -547) and (b) the new model and parameters ($R^2 = 0.93$, MSE = 0.00096 s^{-2} , AIC = -551), plotted against the line of equality (solid black line).

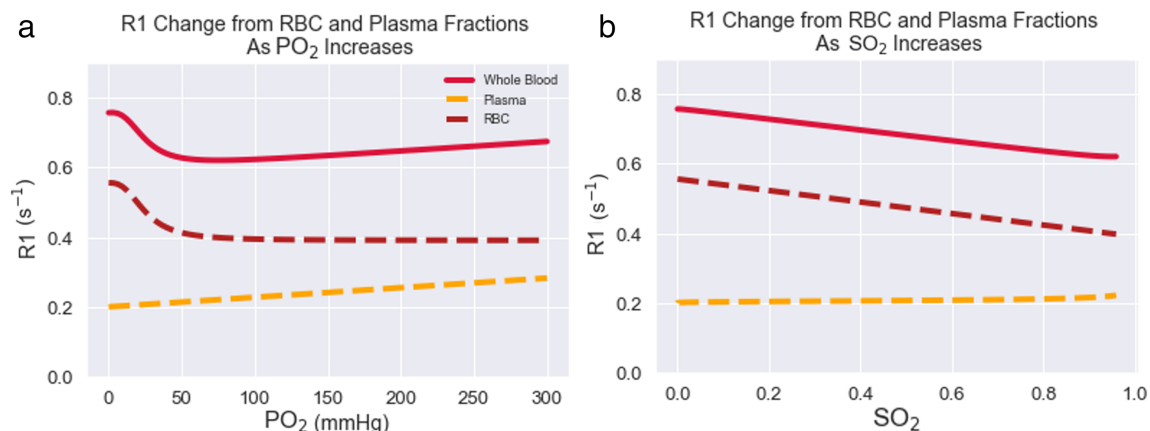


FIGURE 5: Plots with simulated data to illustrate the behavior of the two compartments of the model, the plasma fraction (yellow) and erythrocyte fraction (maroon), as (a) PO₂ increases and (b) SO₂ increases. B₀ = 3 T, Hct = 0.42.

closer agreement with the literature values ($R^2 = 0.93$ vs. 0.92 , $MSE = 0.00096 \text{ s}^{-2}$ vs. 0.00011 s^{-2} for Hales vs. new model, respectively). In addition, the new model was preferred slightly over the Hales model by the AIC criterion, achieving an AIC score of -547 vs. -551 for Hales vs. new model, respectively. The divergence of the predictions of the Hales model vs. the new model as oxygen levels become hyperoxic is shown in Fig. S9 in the Supplemental Material.

The behavior of the erythrocyte and plasma components of the model is shown in Fig. 5, where the model showed that as oxygen levels increased in the blood, the R1 decreased due to the paramagnetic effect of the deoxyhemoglobin fraction, and once full saturation was reached, the predominant remaining effect was the increase in R1 due to the paramagnetic dissolved oxygen in the plasma.

The predicted changes in R1 that would be induced by an increase in oxygen levels are illustrated in Fig. 6a,b, which

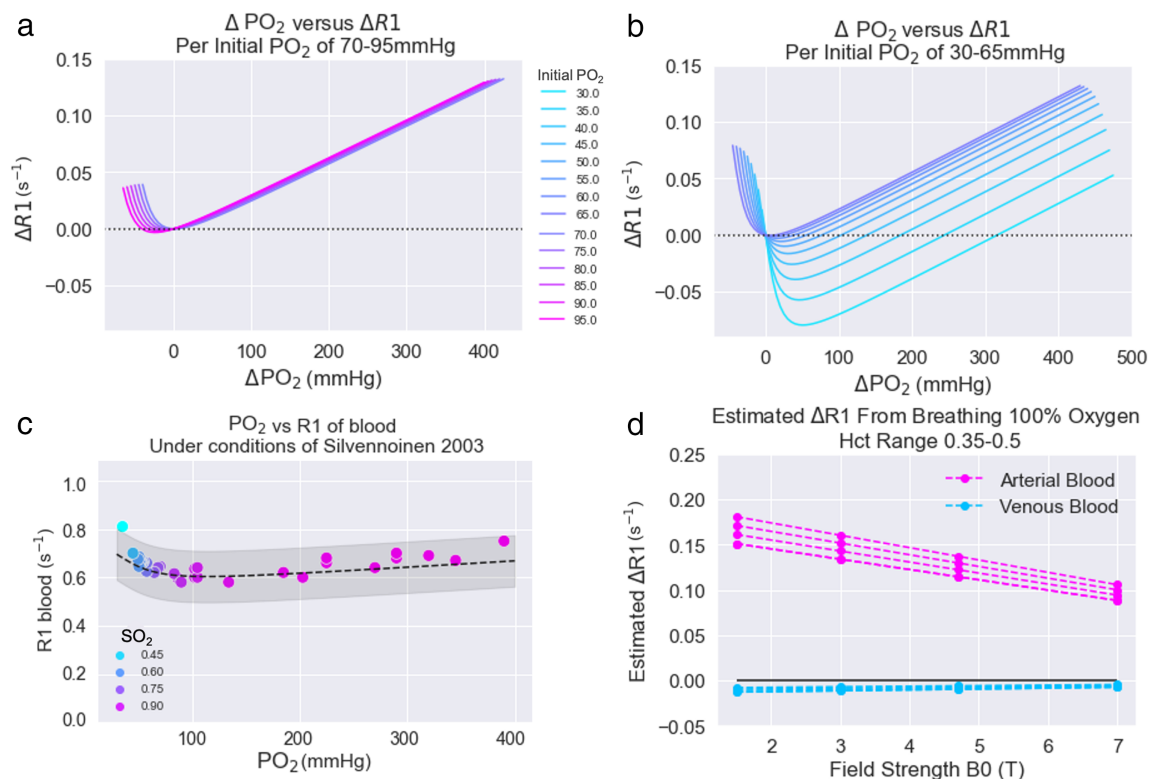


FIGURE 6: Estimated $\Delta R1_b$ as a function of ΔPO_2 (at 3 T and Hct = 0.42) for various initial PO₂ levels of (a) 70–95 mmHg and (b) 20–70 mmHg. The $\Delta R1$ trends match the data shown in (c), which shows the PO₂ vs. R1_b data from Silvennoinen et al⁴ (blue-pink scale is SO₂ level), plotted alongside the R1_b estimated using the new model at the appropriate B₀, Hct, PO₂, and SO₂ (dashed line) with the 95% confidence interval shown in gray. (d) The estimated R1_b in venous and arterial blood after breathing 100% oxygen, based on empirical PO₂ measurements.

shows the so-called “contradictory” negative $\Delta R1$ that has been observed by oxygen-enhanced MRI researchers in hypoxic tumors.^{6–11} As can be seen in Fig. 6c, when starting from a low saturation, the R1 first decreases until full saturation is reached, and then increases linearly with PO_2 . In Fig. 6d, the model showed that a change in PO_2 from 39 mmHg to 48 mmHg (such as in venous blood) induced a negative $\Delta R1$, while a change (such as in arterial blood) from 98 mmHg to 600 mmHg induced a large positive $\Delta R1$.

Effect of W_{RBC} and W_{plasma} Constants

The distribution of resulting R1 values for all combinations of $W_{RBC} = 54\text{--}78\%$ and $W_{plasma} = 94\text{--}96\%$, and $Hct = 0.38\text{--}0.48$ is plotted in Fig. S10 in the Supplemental Material, and the resulting SD of the R1 values for a set hematocrit (range 0.38–0.48) was 0.02 s^{-1} , and a maximum difference of maximum difference in R1 of 0.07 s^{-1} .

Discussion

We have presented a general model to estimate the R1 of blood, accounting for hematocrit, oxygen saturation (SO_2), the partial pressure of oxygen (PO_2), and magnetic field strength under both normal physiological and hyperoxic conditions. The model was valid for the following parameter ranges: $B0 = 1.5\text{--}8.45\text{ T}$, $SO_2 = 0.40\text{--}1$, $PO_2 = 30\text{--}700\text{ mmHg}$, and adjustable for different species by adjusting the P50 constant appropriately. The model estimates agreed well with literature values ($R^2 = 0.93$, $MSE = 0.0013\text{ s}^{-2}$) and the model performance was consistent across R1, SO_2 , PO_2 , B0, and Hct levels.

The new model builds upon a previous model for R1 or T1 of blood,¹⁴ accounting for hematocrit, field strength, and SO_2 , valid between 1.5–7 T and SO_2 of 40–99% (non-hyperoxic conditions). The new model showed improved accuracy and preference within the valid range of the previous model, likely due to the four parameters added which better reflected the true behavior, and also due to a $3\times$ increase in data points available for model fitting. The new model was also valid over a slightly larger range of field strengths (1.5–8.45 T). The main improvement of the new model, however, was that it could account for changes in PO_2 under hyperoxic conditions.

Our model showed that there are two competing effects on blood R1 that arise from increasing oxygen levels (paramagnetic oxygen and paramagnetic deoxyhemoglobin), and that the effect on R1 due to deoxyhemoglobin dominates during lower oxygen levels. O'Connor et al reported that when breathing 100% oxygen, there is a small increase in the venous PO_2 from 39 mmHg to 48 mmHg, while the arterial PO_2 shows a high increase from 98 mmHg to 600 mmHg.³⁹ By modeling these hyperoxic conditions, we were able to quantify the expected $\Delta R1$ in venous and arterial blood after breathing 100% oxygen.

By modeling venous and arterial conditions, this model also provided an explanation for the unexpected additional increase in T1 (decrease in R1) from the oxygen-enhanced drink vs. the control drink reported by Vatnehol et al in the hepatic portal vein, where the authors expected an increase in R1 from increased oxygenation.¹² The authors hypothesized that this contradictory result was due to oxygen increasing the amount of water absorbed into the bloodstream from the beverage and hence increasing the dilution effect.¹² However, according to our model, if the drink increased the oxygen saturation levels in the vein, then a decrease in R1 should be expected—which is consistent with their observations.

As mentioned in the background theory, the R1 of protons in highly mobile molecules such as plasma will be less affected by changing field strength, whereas in low mobility materials (such as protons in biological tissues) the R1 has been empirically shown to decrease as field strength increases.²³ The resulting slope of the field-strength dependence for $R1_p$ (plasma) and $R1_{cox}$ (erythrocytes) agreed well with this theory—the resulting slope for $R1_p$ (i.e., $\beta_{1,R1p}$) was almost 0. In fact, the version of the model with $\beta_{1,R1p}$ set to 0 (i.e., with Eq. 6 set to $R1_p = \beta_{0,R1p}$, hence 7 total parameters) resulted in the highest AIC score and was therefore used in this manuscript. In addition, the removal of the dependence of $R1_{cox}$ produced an extremely low AIC score, therefore suggesting that the R1 of the protons within the erythrocytes was more affected by changing field strength than the R1 of the protons within the plasma, which was consistent with this background theory.

For the purpose of this manuscript, the values used for W_{RBC} and W_{plasma} were 0.70 and 0.95, even though in reality these can range from $W_{RBC} = 54\text{--}78\%$ and $W_{plasma} = 94\text{--}96\%$. When testing the effect of the full range of these variables on R1, it resulted in a maximum difference of 0.07 s^{-1} and SD of 0.02 s^{-1} between any combination of W_{RBC} and W_{plasma} values and set hematocrit, suggesting that deviation from the chosen population average values of 0.70 and 0.95 could account for the remaining variance in the R1 estimate.

Limitations

The R1 values collected were from experiments performed over a timespan of two decades with variation in the experimental equipment and T1-mapping technique used. An accurate measurement of T1 in blood samples or in vivo can be difficult and the measurement accuracy depends on the proper selection of acquisition protocols and parameters (such as repetition and inversion times). Of note, some of the R1 data points collected from Stefanovic et al were underestimated by the model—these were the only data points collected by a Look-Locker T1 mapping method, which are known to overestimate R1.⁴⁰

In addition, a systematic trend in the error distribution by R1 was noticed, however when viewing the datapoints according to the original source, it was apparent that this trend was caused due to the model consistently underestimated the values of R1 reported from one literature source,²⁹ in a way that was not explained by categorization by B0, Hct, SO₂, or PO₂ values. Hueckel et al stated that the temperature of all samples was “approximately 37 °C,” however, inaccuracy in this measurement could have caused a higher R1 than the rest of the authors’ measurements which were performed at 37 °C (or corrected from room temperature).

It is important to note that the values of blood R1 have often been extracted from original plots, some hand-drawn, which is a source of error, and converted from the various original units to s⁻¹/mmHg, which can be another source of error. The hematocrit, SO₂, and PO₂ measurements collected from the literature also have several limitations—eg, it was apparent that researchers tended to report certain rounded values more often than others and to different levels of precision. Altogether, these limitations are a large source of potential error in the accuracy of this model. As a future direction of this work, we have hosted the open-source model code and current R1_b measurements on GitHub (github.com/BulteGroup/R1BloodModel) and invite the MRI community to share more modern measurements of blood R1 at a range of field strengths, hematocrit, SO₂, and PO₂, both in vivo and ex vivo and refit the model to improve accuracy.

The literature dataset used for the model did not include SO₂ values below 40%, so the model may not be valid below that threshold. The Bland–Altman plots showed that the prediction error was greater for a set of data points with lower SO₂ (below 50%). This could be due to the model being slightly less accurate at lower SO₂ due to not having many data points with SO₂ < 50% in the dataset (and none below 40%), or it is possible that these original reported R1 measurements were inaccurate. Regardless, we welcome future researchers to acquire new data points at lower SO₂ and refit the model to re-estimate the parameters and have more certainty within this region if it is desired.

Finally, it should be noted that there are other factors that will influence R1 in blood not included in the model. Plasma proteins that are relevant from an MRI perspective due to either diamagnetism or paramagnetism are albumin, Immunoglobulin G and fibrinogen, transferrin, and ceruloplasmin, and the concentrations of these can differ by age and sex, resulting in a varied plasma R1.²⁸ It is possible that some of the variability in the literature data could be accounted for if these concentrations were also measured and reported. In fact, Li et al have proposed a highly specific model of the R1 of blood accounting for hemoglobin saturation, methemoglobin, and albumin under non-hyperoxic conditions.²¹ These data were not available in the literature used

for the model, but if these were recorded in future studies alongside new R1 measurements they could be utilized for refitting.

Conclusions

In this work, we presented a general model to estimate the R1 of blood, accounting for hematocrit, magnetic field strength, SO₂, and PO₂, under both normal physiological and hyperoxic conditions, and adjustable for different species. This work was built upon a previous model, and we have both improved the accuracy of the R1 estimates within the valid range of the previous model and extended its range of validity to include hyperoxic conditions. Using the predictions of this model, we quantified and explained contradictory oxygen-induced R1 changes reported in the literature and characterized the expected R1 changes arising from the relevant physiological factors.

Acknowledgments

E.B. is supported by funding from the Engineering and Physical Sciences Research Council (EPSRC) and Medical Research Council (MRC) [grant number EP/L016052/1] and the Clarendon Scholarship Fund. D.B. and E.S. also gratefully acknowledge funding from the EPSRC [grant numbers EP/S021507/1 and EP/L024012/1].

References

- Chaganti J, Woodford H, Tomlinson S, Dunkerton S, Brew B. Black blood imaging of intracranial vessel walls. *Pract Neurol* 2021;21:101-107.
- Petcharunpaisan S. Arterial spin labeling in neuroimaging. *World J Radiol* 2010;2:384-398.
- Blockley NP, Jiang L, Gardener AG, Ludman CN, Francis ST, Gowland PA. Field strength dependence of R1 and R2* relaxivities of human whole blood to propanol, vasovist, and deoxyhemoglobin. *Magn Reson Med* 2008;60:1313-1320.
- Silvennoinen MJ, Kettunen MI, Kauppinen RA. Effects of hematocrit and oxygen saturation level on blood spin-lattice relaxation. *Magn Reson Med* 2003;49:568-571.
- d’Othée BJ, Rachmuth G, Munasinghe J, Lang EV. The effect of hyperoxygenation on T1 relaxation time in vitro. *Acad Radiol* 2003;10:854-860.
- Linnik IV, Scott ML, Holliday KF, et al. Noninvasive tumor hypoxia measurement using magnetic resonance imaging in murine U87 glioma xenografts and in patients with glioblastoma. *Magn Reson Med* 2014;71:1854-1862.
- Remmele S, Sprinkart AM, Müller A, et al. Dynamic and simultaneous MR measurement of R1 and R2* changes during respiratory challenges for the assessment of blood and tissue oxygenation. *Magn Reson Med* 2013;70:136-146.
- Yang DM, Arai TJ, Campbell JW, Gerberich JL, Zhou H, Mason RP. Oxygen-sensitive MRI assessment of tumor response to hypoxic gas breathing challenge. *NMR Biomed* 2019;32:e4101.
- Little RA, Jamin Y, Boulton JKR, et al. Mapping hypoxia in renal carcinoma with oxygen-enhanced MRI: Comparison with intrinsic susceptibility MRI and pathology. *Radiology* 2018;288:739-747.

10. Salem A, Little RA, Latif A, et al. Oxygen-enhanced MRI is feasible, repeatable, and detects radiotherapy-induced change in hypoxia in xenograft models and in patients with non-small cell lung cancer. *Clin Cancer Res* 2019;25:3818-3829.
11. Cao-Pham T-T, Joudiou N, Van Hul M, et al. Combined endogenous MR biomarkers to predict basal tumor oxygenation and response to hyperoxic challenge. *NMR Biomed* 2017;30:e3836.
12. Vatnehol SAS, Hol PK, Bjørnerud A, Amiry-Moghaddam M, Haglerød C, Storås TH. Effect of drinking oxygenated water assessed by in vivo MRI relaxometry. *J Magn Reson Imaging* 2020;52:720-728.
13. Desmond KL, Chavez SE. Editorial for "effect of drinking oxygenated water assessed by in vivo MRI relaxometry". *J Magn Reson Imaging* 2020;52:729-730.
14. Hales PW, Kirkham FJ, Clark CA. A general model to calculate the spin-lattice (T1) relaxation time of blood, accounting for haematocrit, oxygen saturation and magnetic field strength. *J Cereb Blood Flow Metab Off J Int Soc Cereb Blood Flow Metab* 2016;36:370-374.
15. Young IR, Clarke GJ, Baffles DR, Pennock JM, Doyle FH, Bydder GM. Enhancement of relaxation rate with paramagnetic contrast agents in NMR imaging. *J Comput Tomogr* 1981;5:543-547.
16. Tripathi A, Bydder GM, Hughes JMB, et al. Effect of oxygen tension on NMR spin-lattice relaxation rate of blood in vivo. *Invest Radiol* 1984;19:174-178.
17. Berkowitz BA, Wilson CA. Quantitative mapping of ocular oxygenation using magnetic resonance imaging. *Magn Reson Med* 1995;33:579-581.
18. Berkowitz BA. Role of dissolved plasma oxygen in hyperoxia-induced contrast. *Magn Reson Imaging* 1997;15:123-126.
19. Zimmerman JR, Brittin WE. Nuclear magnetic resonance studies in multiple phase systems: Lifetime of a water molecule in an adsorbing phase on silica gel. *J Phys Chem* 1957;61:1328-1333.
20. Grgac K, Zijl PCM, Qin Q. Hematocrit and oxygenation dependence of blood $1H_2O$ T1 at 7 tesla. *Magn Reson Med* 2013;70:1153-1159.
21. Li W, Grgac K, Huang A, Yadav N, Qin Q, van Zijl PCM. Quantitative theory for the longitudinal relaxation time of blood water. *Magn Reson Med* 2016;76:270-281.
22. McLaughlin AC, Leigh JS. Relaxation times in systems with chemical exchange: Approximate solutions for the nondilute case. *J Magn Reson* 1969 1973;9:296-304.
23. Rooney WD, Johnson G, Li X, et al. Magnetic field and tissue dependencies of human brain longitudinal $1H_2O$ relaxation in vivo. *Magn Reson Med* 2007;57:308-318.
24. Chou C-Y, Abdesslem M, Bouzigues C, et al. Ultra-wide range field-dependent measurements of the relaxivity of Gd^{3+} -x $EuxVO_4$ nanoparticle contrast agents using a mechanical sample-shuttling relaxometer. *Sci Rep* 2017;7:44770.
25. Elster AD. How much contrast is enough? Dependence of enhancement on field strength and MR pulse sequence. *Eur Radiol* 1997;7: S276-S280.
26. Chu Z, Wang Y, You G, et al. The P_{50} value detected by the oxygenation-dissociation analyser and blood gas analyser. *Artif Cells Nanomed Biotechnol* 2020;48:867-874.
27. Goldman D. Theoretical models of microvascular oxygen transport to tissue. *Microcirculation* 2008;15:795-811.
28. Kindvall S. Pulmonary imaging with quantification of T1-relaxation and oxygen enhanced MRI. Lund University, Faculty of Medicine; 2018.
29. Hueckel P, Schreiber W, Markstaller K, Bellemann M, Kauczor H-U, Thelen M. Effect of partial oxygen pressure and hematocrit on T1 relaxation in human blood. *Proc Int Soc Magn Reson Med* 2000;1586.
30. Lu H, Clingman C, Golay X, van Zijl PCM. Determining the longitudinal relaxation time (T1) of blood at 3.0 tesla. *Magn Reson Med* 2004;52: 679-682.
31. Dobre MC, Ugurbil K, Marjanska M. Determination of blood longitudinal relaxation time (T1) at high magnetic field strengths. *Magn Reson Imaging* 2007;25:733-735.
32. Pilkinton DT, Hiraki T, Detre JA, Greenberg JH, Reddy R. Absolute cerebral blood flow quantification with pulsed arterial spin labeling during hyperoxia corrected with the simultaneous measurement of the longitudinal relaxation time of arterial blood. *Magn Reson Med* 2012;67: 1556-1565.
33. Stefanovic B, Pike GB. Human whole-blood relaxometry at 1.5 T: Assessment of diffusion and exchange models. *Magn Reson Med* 2004;52:716-723.
34. Rane SD, Gore JC. Measurement of T1 of human arterial and venous blood at 7T. *Magn Reson Imaging* 2013;31:477-479.
35. WebPlotDigitizer – Extract data from plots, images, and maps. Available from: <https://automeris.io/WebPlotDigitizer/citation.html>
36. Virtanen P, Gommers R, Oliphant TE, et al. SciPy 1.0: Fundamental algorithms for scientific computing in Python. *Nat Methods* 2020;17: 261-272.
37. Pedregosa F, Varoquaux G, Gramfort A, et al. Scikit-learn: Machine learning in Python. *J Mach Learn Res* 2011;12:2825-2830.
38. Kageyama K, Onoyama Y, Kogawa H, Goto E, Tanabe K. The maximum and minimum water content and cell volume of human erythrocytes in vitro. *Biophys Chem* 1989;34:79-82.
39. O'Connor JPB, Jackson A, Buonaccorsi GA, et al. Organ-specific effects of oxygen and carbogen gas inhalation on tissue longitudinal relaxation times. *Magn Reson Med* 2007;58:490-496.
40. Stikov N, Boudreau M, Levesque IR, Tardif CL, Barral JK, Pike GB. On the accuracy of T1 mapping: Searching for common ground. 2015;73: 514-522.